# Uplift resistance of buried pipelines: the contribution of seepage forces

Revised manuscript submitted to Ocean Engineering

Shubhrajit MAITRA
Research Fellow
Department of Infrastructure Engineering
The University of Melbourne, Victoria 3010, Australia

Former Research Associate
Department of Civil Engineering
Indian Institute of Technology Bombay
Powai, Mumbai – 400 076, India
Email: shubhrajit.maitra@unimelb.edu.au

Santiram CHATTERJEE (corresponding author)
Associate Professor
Department of Civil Engineering
Indian Institute of Technology Bombay
Powai, Mumbai – 400 076, India
Telephone: +91 – 22 – 2576 5327
Email: sc@civil.iitb.ac.in

David WHITE
Professor
Faculty of Engineering and Physical Sciences
University of Southampton,
Southampton SO17 1BJ, UK
Email: david.white@soton.ac.uk

Deepankar CHOUDHURY
Prof. T. Kant Chair Professor and Head
Department of Civil Engineering
Indian Institute of Technology Bombay
Powai, Mumbai – 400 076, India
Email: dc@civil.iitb.ac.in

No. of words: 6752
No. of tables: 1
No. of figures: 13

# Uplift resistance of buried pipelines: the contribution of seepage forces

Shubhrajit Maitra, Santiram Chatterjee, David White and Deepankar Choudhury

## Abstract

Pipelines are commonly buried, and can buckle upwards when heated if there is insufficient soil uplift capacity. Interface tension beneath the buried pipe significantly influences the uplift capacity at shallow embedments. Conventional design approaches, which consider either zero or unlimited interface tension, do not assess and quantify the effect of interface tension on uplift capacity. The present study bridges the gap between conventional "no tension" and "full tension" capacities. Mobilisation of interface tension is governed by seepage forces which in turn directly control the formation of a gap beneath the pipe. A large deformation finite element approach, which simulates this phenomenon of gap formation using a thin layer of gap elements below the pipe, is adopted to study the soil response for various cases of uplift velocity, embedment and soil weight. The enhancement in undrained shear strength of soil at higher uplift velocities due to strain rate effects has also been considered. The interface tension mobilised at these different velocities and embedments varies systematically in a way that is expressed by modifying Hvorslev's intake factors. The proposed expressions may be used with the existing methodologies to assess pipe stability during operation, demonstrated here through a design example.

**Keywords:** Buried pipelines; seepage; soil-structure interaction; uplift capacity; finite element modelling; offshore geotechnics.

**Words:** 6752, **Tables:** 1, **Figures**: 13.

# 1. Introduction

Pipeline systems are an integral part of offshore oil and gas projects as they are used to carry hydrocarbons within the field and also to shore. Offshore pipelines are often buried into the seabed by trenching, particularly in shallow water, to protect them from hydrodynamic wave actions or damage from fishing gear. During operation, these pipes convey oil and gas at high temperature which is significantly higher than the ambient temperature during laying. This results in development of compressive stresses within the pipe, thus making it prone to buckling. For buried pipes, buckling in the upward direction (commonly termed as upheaval buckling) is of predominant concern and is resisted by the soil around and above the pipe. This resistance is influenced by the shear stresses mobilised along slip surfaces, interface tension generated beneath the pipe and the submerged unit weight of the soil.

The peak vertical resistance is termed the uplift capacity per unit length, $V_u$, and estimation of this capacity is essential in designing buried pipeline systems. $V_u$ is often normalised with $s_uD$ (where, $s_u$ is undrained shear strength of the soil and $D$ is diameter of the pipe) to define the non-dimensional bearing factor, $N_u$ (= $V_u/s_uD$). Various types of failure mechanisms can occur during uplift and these are broadly classified into a "global failure mode" and a "local failure mode" (DNV, 2017). In the "global failure mode", the uplift mechanism involves lifting of a wedge of soil along with the pipe and thus, the mechanism extends to the mudline. In the "local failure mode", a localised flow-round mechanism takes place in which soil flows around the pipe resulting in soil movement from top to bottom of the pipe as uplift occurs.

In undrained conditions, theoretical solutions for the uplift resistance of each failure modes exist for idealised cases. Randolph and Houlsby (1984) obtained the limiting values of $N_u$ to be $6+\pi$ ($\approx 9.14$) and $4\sqrt{2}+2\pi$ ($\approx 11.94$) for perfectly smooth and fully rough cylinders respectively, under lateral movement in an infinite medium. These factors are frequently referred to while obtaining undrained uplift factors of deeply embedded pipes because of similar problem geometry. Martin and White (2012) performed numerical limit analyses to study the undrained uplift response for smooth and rough pipes considering extreme cases of interface tension ($T$) and interface roughness coefficient ($\alpha$).

Maitra et al. (2016) proposed a generalized uplift capacity prediction model considering effects of soil heterogeneity and extreme cases of $T$ and $\alpha$. Maitra et al. (2017) further extended the work of Maitra et al. (2016) for studying cases of intermediate interface roughness conditions. Attempts have been made by several other researchers to study uplift response of buried offshore pipelines for various cases of embedment, soil strength profile and unit weight (Zeng et al., 2014; Valle-Molina et al., 2014; Brennan et al., 2017; Charlton and Rouainia, 2019). However, all these previous studies on uplift capacity of buried pipes assume "No Tension" (NT) condition ($T$ = 0) or "Full Tension" (FT) scenario ($T = \infty$) at the pipe-soil interface. As pointed out by Martin and White (2012) and Maitra et al. (2016), uplift capacity can vary to a great degree between the two extremities of $T$, especially for pipes buried at shallow depth. Thus, studying intermediate cases of interface tension becomes important. Pipeline design generally aims to minimise the burial depth as trenching requires huge capital expenditure, so unnecessary conservatism is to be avoided. The present work aims at bridging the gap between the conventionally obtained NT and FT uplift capacities for buried pipes.

During uplift, the mobilisation of interface tension is governed by seepage forces and relies on negative excess pore pressure generated beneath the pipe. This excess pore pressure causes flow of water towards the pipe invert, which results in formation of a water-filled gap beneath the pipe and hence, separation can occur at the bottom of the pipe. This separation is prevented, however, if the overburden stresses cause the effective stress to remain positive, so a gap does not form. This phenomenon of gap formation is commonly termed as "breakaway" (BA). On the other hand, when sufficient interface tension is mobilised, separation at interface cannot occur ("no breakaway" or NBA) and the soil at the bottom interface remains in contact with the pipe. Numerical simulation of this phenomenon of gap formation is challenging and limited attempts have been made by researchers in the past to model the role an opening gap plays on uplift response for various offshore foundations like suction caissons and plate anchors (Cao, 2003; Mana et al., 2014; Thieken et al., 2014; Maitra et al., 2019). From these studies, the factors influencing mobilisation of interface tension have been identified as uplift velocity ($v$), soil permeability ($k$) and shape and size of the foundations. The combined influence of $v$ and $k$ reflects that process is controlled by seepage.

The objective of the present paper is to study the effect of seepage on mobilisation of interface tension beneath a buried offshore pipe by simulating the process of gap formation. A numerical modelling technique has been used here which is similar to that adopted by Maitra et al. (2019) for strip anchors. A series of two-dimensional large deformation finite element (LDFE) analyses were carried out in which the pipe was subjected to displacements at various rates and from the obtained capacities, the contribution of interface tension has been quantified as a function of Hvorslev's intake factors. Also, the strain rate dependency of undrained shear strength of soil has been taken into account while considering various pipe uplift velocities. The proposed model can be incorporated in the design framework proposed by Maitra et al. (2016) and thus, provides a systematic basis for predicting the uplift capacity of buried pipes under a range of uplift conditions spanning between full tension and zero tension. It can also be used to predict buckling behaviour of a buried pipe during its lifetime, illustrated in this paper through a design example.

# 2. Numerical simulation of gap formation

## 2.1 Material model and details of analyses

Notation is defined in Fig. 1. The pipe was considered to be rigid and weightless. Analyses were carried out for three values of $D$ (0.5 m, 1 m, 1.5 m). Results for $D$ = 1 m are the main focus in this paper for brevity, but through non-dimensionalisation the proposed equations can predict the capacities for other values of pipe diameter. Pipe embedment ($w$) was varied to study pore pressure responses for various cases of pipe embedment ratios ($w/D$) ranging from 1.5 to 5.

The material model for soil adopted in the present study is the same as that adopted by Maitra et al. (2019). The soil was considered to be linearly elastic – perfectly plastic porous material and coupled effective stress – pore pressure analyses were carried out. The yield criterion was defined similar to that of Tresca yield criterion, but applied over effective stresses (since, the difference between major and minor principal stresses at failure is the same in total and effective stress space). Carter et al. (1979) had studied a cavity expansion problem considering a similar constitutive relationship and compared the results with that obtained using modified Cam clay model. It was shown that choice of soil model did not influence the pore pressure responses. Since, the primary objective of the current study is to study the breakaway phenomenon associated with seepage, such a simplified constitutive model has been used for modelling soil strength. However, experiments have shown that the soil exhibits fully drained behaviour at $vD/c_v$ less than about ~ 0.01 (Chung et al., 2006), where $c_v$ is the coefficient of consolidation. Thus, at slow uplift rates, the soil is likely to undergo consolidation and may gain in strength, which is not captured using the model considered in the present study. Thus, for the cases of slow uplift, the obtained capacity factors may be on the low, or conservative side.

Detailed studies of uplift response for various shear strength profiles have been carried out by previous researchers (Martin and White, 2012; Maitra et al., 2016) and uplift capacity prediction methodologies exist in the literature for such profiles (DNV, 2017). Also, it has been highlighted by Maitra et al. (2019) that mobilised interface tension depends only on the pull-out rate, soil permeability and problem geometry; and is independent of the soil strength profile. Thus, the focus of the current study is limited to studying the seepage phenomenon during pipe uplift, and effects of soil heterogeneity has not been studied here, but the results are applicable to other soil strength profiles.

The undrained shear strength of the soil has been assumed to be uniform with depth. The Young's modulus, Poisson's ratio and permeability of soil ($k$) are assigned values of $500s_u$, 0.3 and $10^{-7}$ m/s respectively. Three different cases of normalised submerged unit weight of soil have been considered ($\gamma' D/s_u$ = 0, 1 and 2; where, $\gamma'$ is submerged unit of soil) to capture the effect of soil weight on the obtained failure mechanisms at various uplift rates. The effects of strain rate on $s_u$ have also been incorporated in the later part of study using the model suggested by Einav and Randolph (2005) and Zhou and Randolph (2007). In the rate dependent soil model, $s_u$ is expressed as:

$$s_u = s_{u0}\left[1+\mu\log\left\{\max\left(1,\frac{\dot{\gamma}_{max}}{\dot{\gamma}_{ref}}\right)\right\}\right] \quad (1)$$

Here, $\mu$ is the rate effect parameter defined as rate of increase in shear strength per decade and $s_{u0}$ is the $s_u$ measured at a reference shear strain rate ($\dot{\gamma}_{ref}$) of $3\times10^{-6}\,\mathrm{s}^{-1}$. $\mu$ typically varies from 0.05 – 0.2 (Dayal and Allen, 1975; Graham et al, 1983; Biscontin and Pestana, 2001) and thus, three values of $\mu$ in this range (0.05, 0.1 and 0.2) were considered for the effect of strain rate on $s_u$. $\dot{\gamma}_{max}$ is the maximum rate of shear strain which can be obtained using:

$$\dot{\gamma}_{max} = \frac{\Delta\varepsilon_1 - \Delta\varepsilon_3}{\delta_p / D}\frac{v}{D} \quad (2)$$

Here, $\Delta\varepsilon_1$ and $\Delta\varepsilon_3$ are major and minor principal strains respectively, during a small displacement of $\delta_p$ applied to the pipe.

When breakaway occurs, the effective stress at the pipe-soil interface falls to zero and the pipe and soil separate resulting in a gap forming, which is filled with water. Thus, while simulating such phenomenon, volume conservation needs to be maintained, i.e., the gap should grow by a volume equal to the volume of water flowing into it from the adjacent soil. Also, zero effective stress and uniform excess pore pressure conditions should prevail within the gap. These conditions can be numerically simulated by placing a thin gap layer (of initial thickness $t_g$) below the pipe (see Fig. 1). The gap elements should possess the following properties –

(a) Very low stiffness – This ensures that negligible effective stresses are developed within the gap and also, the gap is free to stretch when water flows into it. For this reason, the Young's modulus and Poisson's ratio for the gap elements were assigned values of 1 kPa and 0.01 respectively.
(b) Very high permeability compared to soil – This maintains uniform excess pore pressure condition within the gap. The permeability of the gap layer was set to a very large value (= 1 m/s), i.e., $10^7$ times greater than the permeability of soil.
(c) Small initial thickness – Ideally initial thickness should be zero; however, a small value of $t_g$ is assumed due to numerical constraints. Several initial thicknesses (ranging from $0.01D$ to $0.06D$) and shapes of the gap layer were considered and these were found to have negligible effect on uplift response. An intermediate value $t_g = 0.04D$ was finally chosen to avoid excessively small elements within the gap. The gap layer was defined as the region between two circular arcs (as shown in Fig. 1) having an initial maximum thickness ($t_g$) of $0.04D$ near the pipe invert. Near the leftmost and the rightmost points of the pipe, the thickness of the gap is close to zero and in such places, the geometry of the gap was modified minutely (as shown in Fig. 2) to avoid ill-conditioned elements during the finite element analyses.

For more details on the numerical model and choice of properties for the gap layer, please refer to Maitra et al. (2019). While defining the interaction behaviour at the various interfaces (pipe-soil interface at the top of pipe, pipe-gap and gap-soil interface below the pipe), the "tie" constraint in Abaqus was used which prevents separation between the interacting surfaces.

## 2.2 Large Deformation Finite Element Methodology

The large deformation finite element methodology has been used which is based on "Remeshing and Interpolation Technique with Small Strain" (RITSS) (Hu and Randolph, 1998a, 1998b). Displacement controlled finite element (FE) analyses were performed using a plane strain numerical model constructed in commercial FE software Abaqus (Dassault Systèmes, 2013). The soil and the gap layer were discretized using CPE6MP elements available in Abaqus (6 noded plane strain triangular elements along with pore pressure as degree of freedom). Mesh optimization was carried out to fix the required model dimensions ensuring negligible boundary effects and also to decide on the required mesh densities to minimize errors from numerical approximations. The bottom of the soil domain was restrained from any kind of displacements, whereas vertical displacements were allowed along the side boundaries of the mesh. Zero excess pore pressure boundary conditions were applied to the top boundary of the mesh simulating a seabed surface through which seepage and pore pressure dissipation can occur. Fig. 2 shows an example of a FE mesh for $w/D = 2$.

The pipe was subjected to upward displacements at various rates and several cases of normalised uplift velocities ($v/k$) were considered (ranging from $10^{-2}$ to $10^{4}$) to capture the full range of responses from zero generation of excess pore pressure (fully drained) to zero flow of water beneath the pipe (fully undrained). As part of the LDFE methodology, the entire pipe displacement was broken down into a series of small incremental displacements (= 1% of $D$) and small strain analyses were carried out for each increment. After each increment, the displacements of the boundary nodes were tracked and a new mesh was constructed with the deformed boundaries. Stresses, strains, pore pressures and other field variables were mapped from the deformed mesh to the reconstructed new mesh before applying the next displacement increment. While pore pressures were mapped for the entire soil and gap elements, stresses were mapped for the soil domain only. The effective stresses developed inside the gap were readjusted to zero after each increment to simulate a water-filled gap realistically. This is essential in modelling the breakaway phenomenon and has been highlighted by Maitra et al. (2019).

The undrained shear strength of the soil was updated after every iteration using the model described using Eqs. (1) and (2) to incorporate the effects of strain rate. The mapping of these field variables as well as pre- and post-processing were done using subroutines written in Fortran and scripts written in Python.

## 2.3 Benchmarking of the adopted methodology

When a pipe undergoes uplift at a very slow rate, negative excess pore pressure developed below the pipe is negligible and a "No Tension" ($T$ = 0) condition prevails at the interface. On the other hand, for very high uplift velocity, there is no water flow beneath the pipe and large amounts of negative excess pore pressure can be generated, which corresponds to the "Full Tension" ($T = \infty$) scenario. Thus, the uplift capacity factors ($N_u = V_u/s_uD$) obtained from the present study for the smallest $v/k$ (= 0.01) can be benchmarked against the NT uplift factors generated by Martin and White (2012) and Maitra et al. (2016). $N_u$ corresponding to $v/k$ = $10^4$ for various $w/D$ can be benchmarked with the FT factors from the same studies, but with the following caveat (see Fig. 3).

It is important to recognise that the gap elements have a low shear strength, representative of a 'smooth' interface ($\alpha \rightarrow 0$), which influences the fully undrained uplift resistance. Martin and White (2012) and Maitra et al. (2016) obtained uplift factors for cases of $\alpha$ = 0 and 1 around the full periphery of the pipe. In the present numerical model, the top surface of the pipe is "tied" to the soil so it behaves as a rough interface, whereas the bottom of the pipe is “tied” to the “soft” gap layer and thus, the interaction surface at bottom of the pipe is equivalent to smooth. Thus, the FT uplift resistance in the present work corresponds to an overall intermediate roughness ($0 < \alpha < 1$) in previous work.

For all $w/D$, the obtained uplift factors for $v/k = 0.01$ lie between the NT factors obtained by earlier researchers for smooth and rough pipes, whereas $N_u$ obtained at $v/k = 10000$ falls in between the FT factors corresponding to $\alpha = 0$ and 1 (Fig. 3). This shows a good agreement between the obtained uplift factors using the present numerical model, plasticity theory solutions and the existing design methodology for extreme cases of interface tension.

Based on upper bound limit analysis by Martin and Randolph (2006), the limiting uplift factor ($N_{u(limit)}$) for deeply embedded pipe in weightless soil is close to 10.8 for $\alpha = 0.5$. Also, Thusyanthan et al. (2008) carried out tests in a geotechnical centrifuge to study uplift resistance in clayey backfill and reported an uplift capacity factor of 10.5 during fast pull out at 0.2 mm/s for $w/D = 5$, 6. Thus, the limiting uplift factor ($N_{u(limit)}$) obtained in this study (for e.g., $N_u \approx 10.6$ for $w/D = 5$, $v/k = 10^4$ in Fig. 3) is consistent with the findings from these previous studies.

# 3. Results and discussions

## 3.1 Uplift response at various uplift rates for $\mu = 0$ (No rate effect)

Figs 4a and 4b show the mobilisation of uplift resistance with pipe displacement for $w/D = 2$ and 4. The mobilisation displacements (taken as displacement required for mobilising 95% of the peak uplift resistance) for various cases considered in this study were found to range between 3% to 10% of $D$. Larger mobilisation displacements were required for pipes placed at deeper embedment depths (markers in Figs. 4a and b indicate that this displacement is ~ $0.05D$ and ~$0.08D$ for $w/D = 2$ and 4 respectively). Figs. 4c and d show the variation in obtained uplift capacity factors ($N_u = V_u/s_uD$) with $v/k$ and $\gamma'D/s_u$ for $w/D = 2$, 4 ($D = 1$ m). The results are plotted in this manner since the uplift velocity was the input to the numerical analyses, rather than the mobilised uplift resistance. However, the results could equally be interpreted as the uplift rate in response to a particular level of applied force, generated by the heating of the pipeline or any other action. If the applied force lies below the NT capacity, then the pipe will remain stationary in equilibrium. If the applied force exceeds the FT capacity, then the pipeline will move upwards, breaking out in an uncontrolled manner. For intermediate levels of mobilised uplift resistance, the pipe will move upwards at the rate $v/k$ given by the responses shown in Fig. 4.

The increase in $N_u$ with $v/k$ reflects the mobilisation of interface tension that depends on generation of negative excess pore pressures underneath the pipe. This bridging of the gap between the conventional NT and FT capacities is the primary objective of the study.

As highlighted by Martin and White (2012) and Maitra et al. (2016), uplift capacity under NT conditions increases with increase in soil weight by an amount equal to the weight of the soil column lying above the pipe (provided the capacity does not exceed the FT capacity). This aspect is evident in Fig. 4c, as $N_u$ increases in proportion to $\gamma'D/s_u$ for $v/k = 0.01$. On the other hand, under FT conditions, $N_u$ decreases with an increase in $\gamma'D/s_u$ because the submerged weight of soil displaced by pipe (referred to in pipeline geotechnics as the soil buoyancy force, e.g. DNV 2017)) assists in uplift when breakaway cannot occur. This leads to a reduction in capacity by $\gamma'A_s$, where $A_s$ is the area of the pipe cross-section (this reduction is analogous to the buoyancy effect in fluid, except in this case soil acts as the weighty material that is displaced).. Thus, $N_u$ reduces with increasing $\gamma'D/s_u$ at $v/k = 1000$. As a result, with increasing $\gamma'D/s_u$, the NT and FT capacities converge. Also, the FT capacities do not increase beyond a certain embedment (see Fig. 3) when the mechanism becomes fully localised and limiting conditions are reached. Hence, the NT capacity converges towards the FT capacity with increase in $w/D$ as well. Thus, with increase in $w/D$ and/or $\gamma'D/s_u$, the uplift capacity under NT and FT conditions eventually become equal (see $N_u$ for $\gamma'D/s_u = 2$ and $w/D = 4$ in Fig. 4d). For these cases $N_u$ becomes independent of the uplift velocity, and a water-filled gap cannot form beneath the pipe.

Some examples of failure mechanisms after a pipe displacement of $0.15D$ are shown in Fig. 5 for $v/k$ = 10, 100; $w/D$ = 2, 4; and $\gamma'D/s_u$ = 0, 2. These cases correspond to the various data points labelled in Figs. 4c and d. Fig. 5 illustrates the transition in uplift mechanism for varying $v/k$, $w/D$ and $\gamma'D/s_u$. The gap elements are not included in the contours and instead are left white to show the gap. Here, the soil displacements ($u_{soil}$) are normalised by the displacement of the pipe ($u_{pipe}$). For pipes buried at shallow embedments, breakaway (or gap formation) can occur only when (a) uplift occurs at a sufficiently slow rate to prevent excess pore pressures and interface tension being mobilised below the pipe, so that the gap grows as water flows into it; and (b) overburden stresses are low enough to allow a stable gap to be formed beneath the pipe, at zero effective stress. Thus, for a shallow pipe displacing at a slow velocity in soils with low $\gamma'D/s_u$ (see Fig. 5a), breakaway occurs and a nearly vertical column of soil is uplifted as the pipe displaces – which is a global failure mode, in the terminology of DNV (DNV, 2017).

The soil flow of Fig. 5a is the same as the NT case, with soil movement only occurring above the pipe. However, the uplift resistance is $N_u$ = 7, which significantly exceeds the NT resistance of 2.5. The additional resistance is from tension on the underside of the pipe, which arises from negative excess pore pressures that cause seepage into the gap as the pipe moves upwards.

For higher values of $v/k$ (compare Fig. 5a and c), gap formation is not feasible and thus, the mechanism extends between the top and bottom of the pipe resulting in a reverse bearing (or two-sided) mechanism. From Fig. 5b, it can be seen that breakaway may not be possible even at slow uplift rate for a shallowly buried pipe in soil with high $\gamma'D/s_u$ because of the effect of soil weight. Fig. 5a to d shows failure mechanisms extending to the seabed for $w/D = 2$, resulting in a global failure mechanism.

With increasing embedment, a local failure mechanism is more common (see Fig. 5f to h). Breakaway is less likely to occur for such cases as higher embedment not only implies higher overburden stresses but also involves a longer seepage flowpath as the distance from the seabed increases. This leads to a more rapid increase in interface tension with increase in $v/k$. For cases where NT and FT capacities are equal (e.g., $\gamma'D/s_u = 2$ and $w/D = 4$ in Fig. 4d), the mechanism is identical at all uplift velocities (compare Fig. 5f and h). Fig. 5e shows a typical intermediate mechanism involving a combination of lifting of soil above the pipe and a partial local flow-round mechanism. Thus, the transition in mechanism from "breakaway" to "no breakaway" is well captured in the figure.

Fig. 6 shows the excess pore pressure diagrams (defined relative to the hydrostatic in-situ pore pressures) corresponding to the cases considered in Fig. 5. These illustrate how the interface tension is linked to the generation of negative excess pore pressures beneath the pipe. With increasing $v/k$, higher negative excess pore pressures are generated near the pipe invert (compare Fig. 6a and c, Fig. 6e and g) which leads to higher uplift resistance at faster uplift rates.

For a particular uplift rate, higher negative excess pore pressures are generated for deeper embedments as the flowpath length increases (compare Fig. 6a and e). However, this is not always true (compare Fig. 6c and g) because the difference between NT and FT capacities reduces with increase in embedment. Thus, the amount of interface tension required to mobilise the limiting resistance (i.e., FT capacity) reduces with increasing embedment. There is no increase in negative excess pore pressures with $v/k$ once FT conditions are reached. For the case where NT and FT capacities are equal in Fig. 4d ($\gamma'D/s_u = 2$ and $w/D = 4$), the negative excess pore pressure mobilised throughout the entire soil domain is close to zero at all uplift velocities (see Fig. 6f and h). In such case, a gap does not form even at the lowest uplift rate as the effective stress remains positive beneath the pipe, so breakaway is not feasible.

## 3.2 Hvorslev's intake factors for buried pipes placed at various *w*/*D*

The amount of interface tension that is generated beneath a strip anchor has been solved by Maitra et al. (2019) using Hvorslev's general equation, which was originally used to model seepage into the base of a borehole (Hvorslev, 1951). The same approach can also be applied to quantify the component of $V_u$ that is additional to the NT limit, and is created by seepage and the resulting tension beneath the pipe. This extra resistance, $V_{seepage}$, can be expressed as:

$$V_{seepage} = \left(\frac{\gamma_w D^2}{F}\right)\left(\frac{v}{k}\right) \tag{3}$$

where, $\gamma_w$ is the unit weight of water, $F$ is Hvorslev's intake factor, which is a non-dimensional geometric factor that primarily depends on the flow geometry, boundary condition and permeability anisotropy of the soil. Several researchers have derived $F$ for various problem geometries (Wilkinson, 1968; Brand and Premchitt, 1980a, 1980b; Ratnam et al., 2001; Maitra et al., 2019). In the present study, $F$ has been obtained for various cases of $w/D$ (see Figs. 7 and 8) using curve fitting by the method of least squares for minimisation of errors.

Fig. 7a shows that $F$ is independent of $s_u$, because the same value captures the effect of interface tension for various $s_u$ values for $w/D$ = 2. Fig.7b highlights that $F$ is independent of $D$, provided $w/D$ remains the same (for $w/D$ = 2, $F$ is obtained as 2.2 for both $D$ = 0.5 m and 1 m). Thus, $F$ is therefore a geometric constant governed only by the geometry of the flow field. $V_u$ obtained for various cases of $w/D$ and $v/k$ are plotted in Fig. 7c (see markers) for weightless soils. Using the $F$ obtained for each $w/D$, $N_u$ is predicted for various embedment ratios using Eq. (4) (see lines in Fig. 7c).

$$V_u = V_{NT} + V_{seepage} \le V_{FT} \tag{4}$$

where $V_{NT}$ and $V_{FT}$ are the uplift capacities under NT and FT conditions respectively, and $V_{seepage}$ is calculated using Eq. (3). Good agreement between the numerical and predicted factors is evident, comparing markers with lines.

Maitra et al. (2016) proposed a prediction methodology for estimating $V_{NT}$ and $V_{FT}$ considering various shear strength profiles and extreme values of interface roughness. In the current study, $V_{NT}$ and $V_{FT}$ are estimated corresponding to $v/k = 10^{-2}$ and $10^4$ respectively. Soil non-homogeneity has not been considered in the present study, but $V_{seepage}$ is independent of the $s_u$ profile. The expression for $V_{seepage}$ proposed here can be used in conjunction with the uplift resistance prediction methodology proposed by Maitra et al. (2016) to estimate $V_u$ at various uplift rates in non-homogeneous soils as well.

Comparing results for different embedments, it is evident that $F$ is a function of $w/D$ (Fig. 8). This is because larger negative excess pore pressures (and hence, higher $V_{seepage}$) are developed for a given $v/k$ at deeper embedments as the seepage path becomes longer with the increase in depth. An equation that relates $F$ to $w/D$ is obtained using curve fitting (see Fig. 8) by method of least squares as follows:

$$F = \frac{1.45}{1 - \exp\left[-0.55\left(w/D\right)\right]} \tag{5}$$

### 3.3 Effects of strain rates on uplift capacity

While considering a range of uplift rate, it becomes important to consider the strain rate dependency of $s_u$ and its effect on the uplift capacity. The rate dependent soil model expressed in Eq. (1) has been used for this purpose and has been implemented using the LDFE framework (see section 2.2). The rate effect parameter, $\mu$ has been varied over a wide range while obtaining $V_u$ for various cases of $v/k$, $w/D$ and $\gamma'D/s_u$. Fig. 9 shows the obtained uplift capacity factors ($V_u/s_{u0}D$) at various uplift rates for $w/D$ = 2, 4 and $\mu$ = 0, 0.05, 0.1 and 0.2 in weightless soil. Here, $s_{u0}$ is $s_u$ measured at a reference strain rate given earlier. For $\mu > 0$, $V_u$ increases significantly at higher uplift rates (even after FT conditions are attained) which can be attributed to the viscous effects of soil flow leading to increase in $s_u$ with increasing $v/k$.

The increase in $s_u$ at high $v/k$ can be captured using the approach of estimating $s_{u,eff}$ (as suggested by Chatterjee et al., 2012; Ghorai and Chatterjee, 2017), where $s_{u,eff}$ is the effective or equivalent shear strength considering rate effect. $s_{u,eff}$ is expressed as:

$$s_{\mathrm{u,eff}} = s_{\mathrm{u0}}\left[1+\mu\log\left\{\max\left(1,\frac{f_{\mathrm{r}}v}{D\dot{\gamma}_{\mathrm{ref}}}\right)\right\}\right] \tag{6}$$

Here, $f_r$ indicates the average operative shear strain rate and is found to be 0.8 using curve fitting in the present study. On normalising $V_u$ with respect to $s_{u,eff}D$, the various sets of curves corresponding to various $\mu$ (see Fig. 9) reduces to a narrow band for each embedment ratio (compare markers with lines in Fig. 10). This approach helps in capturing the effects of strain rate on uplift resistance.

## 4. Proposed design framework considering effects of interface tension and strain rates

Maitra et al. (2016) proposed a prediction methodology for estimating uplift capacity of buried pipes under FT and NT conditions. A brief overview of this methodology is provided herein for better understanding. $V_{FT}$ and $V_{NT}$ can be predicted using Eqs. (7) and (8) respectively.

$$V_{\mathrm{FT}} = \left[N_{\mathrm{u0}} + \left(N_{\mathrm{u(limit)}} - N_{\mathrm{u0}}\right)\left\{1-\exp\left(-0.4\left(w/D\right)^{\beta_1}\right)\right\}\right]s_{\mathrm{u,eff}}D - \gamma' A_{\mathrm{s}} \tag{7}$$

$$V_{\mathrm{NT}} = N_{\mathrm{u(limit)}}\left(1-\frac{1}{1+0.2\left(\dfrac{w}{D}-0.5\right)^{\beta_2}}\right)s_{\mathrm{u,eff}}D + \gamma'\left[\left(w-D\right)D + D^2\left(\frac{1}{2}-\frac{\pi}{8}\right)\right] \tag{8}$$

The first part of each of these equations quantifies the geotechnical resistance from soil due to its shear strength, whereas the later part captures the effect of soil weight on uplift capacity.

$N_{u0}$ is the normalised uplift factor in weightless soil under FT conditions for $w/D \rightarrow 0$. $\beta_1$ and $\beta_2$ are empirical curve-fitting parameters. Please refer to Maitra et al. (2016) for the values of the parameters $N_{u0}$, $N_{u(limit)}$, $\beta_1$ and $\beta_2$; and for more details on the procedure for estimating $s_{u,eff}$ for a generalised $s_u$ profile.

The results from the present study can be used in tandem with this existing methodology for predicting capacity over the entire range of interface tension, spanning through the zone where seepage forces lead to intermediate levels of uplift resistance. A summary of the methodology is as follows:

(a) The capacity under NT and FT conditions ignoring seepage can be estimated using Eqs. (7) and (8). The effects of soil shear strength heterogeneity can be incorporated using this approach. While calculating $s_{u,eff}$, the effects of strain rate may be integrated into the methodology using Eq. (6).

(b) Hvorslev's intake factor, $F$ and the seepage component of uplift capacity, $V_{seepage}$ can be obtained using Eqs. (5) and (3) respectively.

(c) Finally, the uplift capacity for a particular $v/k$ can be estimated using Eq. (4).

If seepage occurs, due to an uplift resistance, $V_u$, greater than $V_{NT}$ being mobilised, then the embedment of the pipe will progressively reduce over time, under a constant applied $V_u$. This reduction in embedment causes a corresponding reduction in both $V_{NT}$ and $V_{FT}$, and therefore an increase in the mobilised seepage force, $V_{seepage}$, and the seepage velocity, $v$. At a shallow embedment, $V_{FT}$ may fall below $V_u$ and the failure mechanism will change to full tension, rather than seepage flow. During this progressive seepage process, the pipe uplift response can be represented by the mechanical analogue system shown in Fig. 11, which is in a format suitable for inclusion in structural models of pipeline upheaval buckling. The conventional uplift capacities $V_{NT}$ and $V_{FT}$ are represented as plastic sliders, while the seepage force is a damper, with resistance proportional to velocity. The slider and damper coefficients are found via the expressions described above, which are dependent on embedment and therefore would need updating as a structural analysis progresses and the pipe moves upwards.

## 5. Design example on prediction of buckling behaviour of a buried pipe

To illustrate the resulting structural response of a pipe subjected to uplift force and seepage, we now introduce a simplified representation of the uplift loading imposed on the soil backfill by the pipeline within an upheaval buckle.

Palmer et al. (1990) demonstrated a conceptual design method to analyse the stability of a buried pipe in operation. During laying of a pipe by trenching, imperfections are introduced into the pipe profile. The downward force (*V*) needed for equilibrium of a pipe under an axial compressive force (*P*) has been expressed by Palmer et al. (1990) using a maximum download parameter ($\Phi_w$) and a dimensionless imperfection length, $\Phi_L$ as follows:

$$\Phi_w = V \times EI / \delta P^2 \tag{9}$$

$$\Phi_L = L\left(P / EI\right)^{0.5} \tag{10}$$

Here, *EI* is the flexural rigidity of the pipe and $\delta$ is the height of imperfection over a length, *L*. A universal design curve has been proposed by Palmer et al. (1990) (see Fig. 12) for assessing pipe stability under operation. A point lying above the universal design curve indicates a pipe that is in a stable equilibrium position, whereas a point lying below this curve implies instability. This simplified analytical model can be used in an incremental form to predict the behaviour of a buried pipe carrying hydrocarbon at a certain operating temperature. A design example is demonstrated in this section that illustrates this. Since, uplift capacity is mobilised at very small pipe displacements, the analytical model presented here assumes that peak resistance is mobilised at the instance the pipe starts displacing.

In this design example, a steel pipe having a diameter of 0.35 m, wall thickness of 0.02 m and embedded at $w/D$ = 3 is considered. Young's modulus and coefficient of thermal expansion for the pipe material were taken as 210 GPa and 1.2 × $10^{-5}$/°C respectively, which are representative values for steel. The submerged operational weight of the pipe was assumed as 1.2 kN/m. The length and height of imperfections, which are formed during pipe laying, were considered as 15 m and 0.25 m respectively. A normally consolidated clayey seabed is considered with typical values of $s_u$, $\gamma'$ and $k$ as follows: $s_u = 1.5z$ (where, $z$ is depth below mudline in metres), $\gamma' = 4$ kN/m$^3$ and $k = 10^{-8}$ m/s.

Table 1 shows list of various input parameters and calculation steps for an operational temperature ($\Delta T$) of 70°C (measured in excess of in-situ temperature). In this example, axial compressive stress has been calculated considering effects of thermal expansion only. In reality, axial stresses can also be generated due to other factors (e.g., internal pressure from hydrocarbons) and a designer should consider these aspects as well while estimating axial compressive force. After estimating the thermal compressive force developed on the pipe, the design method by Palmer et al. (1990) has been used to estimate the downward force, $V$ required for the pipe to be in equilibrium. $V$ is estimated as 3.63 kN/m (using Eqs. 10 and 9) and thus, the uplift resistance that needs to be mobilised for equilibrium is $V - W' = 2.43$ kN/m, where $W'$ is submerged operational weight of pipe. For this particular case, the NT and FT uplift capacities are obtained as 2.034 kN/m and 4.442 kN/m respectively using the approach proposed by Maitra et al. (2016) and Maitra et al. (2017). Since $V - W'$ exceeds $V_{NT}$ (see Fig. 12), interface tension and seepage forces are mobilised (by an amount $V - W' - V_{NT}$) which corresponds to an initial uplift velocity of 0.51 mm/day (obtained using Eq. 3). The solution presented here has been integrated over time (considering small time increments) to obtain the pipe displacements and velocities over a period of time. Calculations are repeated for other values of $\Delta T$ ranging from 65°C to 85°C and the results are presented in see Fig. 13. As the pipe displaces in the upward direction, $V_{NT}$ reduces due to the presence of weaker soil at shallow depth and the reduction in embedment ratio. As a consequence, there is an increase in seepage forces leading to acceleration of the pipe. As is evident from the figure, upheaval occurs rapidly at higher operating temperatures, whereas the pipe may not displace at all at low operating temperatures (for e.g., $\Delta T$ = 65°C in Fig. 13). Thus, the design example presented here illustrates the prediction of buckling behaviour of an offshore pipe in operation and can be used to assess the allowable operational temperatures and time periods for a buried pipe. This solution is based only on the Palmer solution for the required uplift force, but the same approach could be integrated into a full structural model of an upheaval buckle via the mechanical analogue system shown in Fig. 11.

The design example presented here showcases calculations for certain values of parameters. However, these parameters (e.g., $s_u$ profile, $k$, $\gamma'$, imperfection height and length) can vary widely along the length of a pipeline and thus, a designer should consider these aspects as well in a real offshore project. It should be noted that pipelines are usually buried inside trenches and the backfill soil may have cracks or openings within it, which in turn can influence the seepage flowpath. The readers should be aware that the design example presented here is based on an idealised soil profile and does not consider these aspects.

# 6. Conclusions

The uplift resistance of buried pipelines is affected by the potential for tension to be mobilised beneath the pipe, associated with seepage into a gap. In the present study, this breakaway phenomenon has been numerically simulated to quantify the role of seepage and interface tension on the uplift resistance for buried offshore pipelines. The large deformation finite element methodology has been used with a thin gap layer below the pipe to ensure volume conservation during flow. Several cases of pipe embedment ratio and normalised unit weight of soil have been considered to obtain the uplift capacity over wide ranges of normalised uplift velocity in soils with uniform undrained shear strength.

From the obtained results, the additional resistance from interface tension and seepage has been expressed analytically using Hvorslev's intake factor, which is a geometric constant that depends solely on embedment ratio. Uplift capacity is then expressed simply as the summation of "No Tension" capacity and the additional component from interface tension and seepage, provided it does not exceed the "Full Tension" capacity which is the upper limit. The effects of strain rate on $s_u$ at various uplift rates have also been studied and an approach for calculating the effective shear strength at high uplift rates has been incorporated.

The proposed model from the present study may be used in accompaniment with the prediction framework proposed by Maitra et al. (2016) to estimate uplift capacity in non-homogeneous soils as well. A design example is presented at the end which illustrates the application of the present study towards analysing the buckling behaviour of a buried pipe during its lifetime. The time to upheaval failure for different operational temperatures can be assessed. The analysis shows that in low permeability soils, or if only small levels of seepage force are mobilised, the pipe can remain embedded for many weeks despite the no-tension uplift capacity being exceeded and ongoing seepage. In more onerous conditions, the analysis shows the rate at which the pipeline movement will accelerate as failure is approached.

The present work does not incorporate the potential for soil strength enhancement due to consolidation, which may be significant at slow uplift rates. This is a limitation of the proposed model which therefore provides conservative low estimates of uplift capacity in situations where consolidation would be significant. Also, Hvorslev's intake factor is estimated for $w/D$ ranging from 1.5 to 5, and thus, extrapolating $F$ beyond this range of $w/D$ needs to be done with caution.

Overall, the outcome of the current study is to bridge the gap between the conventional no-tension and full-tension uplift capacities that are wide apart for pipes buried at shallow depths. The results allow estimates to be made of the uplift rate when intermediate levels of uplift resistance are mobilised, which is a significant contribution to current design practices.

## Acknowledgements

The authors are grateful to the Australia-India Council, Department of Foreign Affairs and Trade, Australian Government for the financial support (grant number AIC122-2015) to initial this collaborative research. The work was initiated between the University of Western Australia (UWA) and the Indian Institute of Technology Bombay, India, when the third author was based at UWA.

## Notation

$A_s$ Cross-sectional area of the pipe

$c_v$ Coefficient of consolidation

$D$ Pipe diameter

$E$ Young's modulus of pipe material

$F$ Hvorslev's intake factor

$f_r$ Operative rate of shear strain

$I$ Moment of inertia

$k$ Permeability of soil

$L$ Length of the pipe

$N_u$ Uplift capacity factor

$N_{u(limit)}$ Limiting value of $N_u$ under "Full Tension" conditions

$N_{u0}$ $N_u$ under "Full Tension" conditions for $w/D \rightarrow 0$

$P$ Axial compressive force acting on the pipe cross-section

$s_u$ Undrained shear strength of soil

$s_{u0}$ $s_u$ measured at reference shear strain rate

$s_{u,eff}$ Effective or equivalent undrained shear strength of soil

| | |
|---|---|
| $T$ | Interface tension |
| $t_g$ | Initial thickness of gap layer |
| $u_{pipe}$ | Displacement applied to pipe |
| $u_{soil}$ | Displacement of soil |
| $V$ | Downward force needed for pipe equilibrium |
| $V_u$ | Uplift capacity |
| $v$ | Uplift velocity |
| $V_{FT}$ | Uplift capacity under "Full Tension" conditions |
| $V_{NT}$ | Uplift capacity under "No Tension" conditions |
| $V_{seepage}$ | Seepage component of uplift capacity |
| $w$ | Embedment depth of pipe invert |
| $\alpha$ | Interface roughness coefficient |
| $\beta_1, \beta_2$ | Empirical curve-fitting parameters for obtaining $V_{FT}$ and $V_{NT}$ |
| $\Delta\varepsilon_1$ | Major principal strain |
| $\Delta\varepsilon_3$ | Minor principal strain |
| $\delta$ | Height of imperfection |
| $\delta_p$ | Small incremental displacement applied to pipe |
| $\gamma_w$ | Unit weight of water |
| $\gamma'$ | Submerged unit weight of soil |
| $\dot{\gamma}_{max}$ | Maximum rate of shear strain |
| $\dot{\gamma}_{ref}$ | Reference shear strain rate |
| $\mu$ | Rate effect parameter defined as rate of increase in $s_u$ per decade |
| $\Phi_L$ | Dimensionless imperfection length |
| $\Phi_w$ | Maximum download parameter |

## References

Biscontin, G., Pestana, J.M., 2001. Influence of peripheral velocity on vane shear strength of an artificial clay. Geotech. Test J. 24 (4), 423-429. https://doi.org/10.1520/GTJ11140J.

Brand, E.W., Premchitt, J., 1980a. Shape factors of cylindrical piezometers. Géotechnique 30 (4), 369-384. https://doi.org/10.1680/geot.1980.30.4.369.

Brand, E.W., Premchitt, J., 1980b. Shape factors of some non-cylindrical piezometers. Géotechnique 30 (4), 536-537. https://doi.org/10.1680/geot.1980.30.4.536.

Brennan, A.J., Ghahremani, M., Brown, M.J., 2017. Strength reduction for upheaval buckling of buried pipes in blocky clay backfill. Ocean Eng. 130, 210-217. https://doi.org/10.1016/j.oceaneng.2016.12.006.

Cao, J., 2003. Centrifuge modeling and numerical analysis of the behaviour of suction caissons in clay. Ph.D. thesis. Memorial University of Newfoundland, Canada.

Carter, J.P., Randolph, M.F., Wroth, C.P., 1979. Stress and pore pressure changes in clay during and after the expansion of a cylindrical cavity. Int. J. Numer. Anal. Met. Geomech. 3 (4), 305-322. https://doi.org/10.1002/nag.1610030402.

Charlton, T.S., Rouainia, M., 2019. Probabilistic analysis of the uplift resistance of buried pipelines in clay. Ocean Eng. 186, 105891. https://doi.org/10.1016/j.oceaneng.2019.03.041.

Chatterjee, S., White, D.J., Randolph, M.F., 2012. The effects of penetration rate and strain softening on the vertical penetration resistance of seabed pipelines. Géotechnique 62 (7), 573-582. https://doi.org/10.1680/geot.10.P.075.

Chung, S.F., Randolph, M.F., Schneider, J.A., 2006. Effect of penetration rate on penetrometer resistance in clay. J. Geotech. Geoenvironmental Eng. 132 (9), 1188-1196. https://doi.org/10.1061/(asce)1090-0241(2006)132:9(1188).

Dassault Systèmes, 2013. Abaqus 6.13 analysis user's manual. Dassault Systèmes.

Dayal, U., Allen, J.H., 1975. The effect of penetration rate on the strength of remolded clay and sand samples. Can. Geotech. J. 12 (3), 336-348. https://doi.org/10.1139/t75-038.

DNV, 2017. Pipe-soil interaction for submarine pipelines. Recommended Practice DNVGL-RP-F114. Det Norske Veritas (DNV), Norway.

Einav, I., Randolph, M.F., 2005. Combining upper bound and strain path methods for evaluating penetration resistance. Int. J. Numer. Meth. Eng. 63 (14), 1991-2016. https://doi.org/10.1002/nme.1350.

Ghorai, B., Chatterjee, S., 2017. Influences of strain rate and soil remoulding on initial break-out resistance of deepwater on-bottom pipelines. Comput. Geotech. 91, 82-92. https://doi.org/10.1016/j.compgeo.2017.07.006.

Graham, J., Crooks, J.H., Bell, A.L., 1983. Time effects on the stress-strain behaviour of natural soft clays. Géotechnique 33 (3), 327-340. https://doi.org/10.1680/geot.1983.33.3.327.

Hu, Y., Randolph, M.F., 1998a. A practical numerical approach for large deformation problems in soil. Int. J. Numer. Anal. Met. Geomech. 22 (5), 327-350. https://doi.org/10.1002/(SICI)1096-9853(199805)22:5%3C327::AID-NAG920%3E3.0.CO;2-X.

Hu, Y., Randolph, M.F., 1998b. H-adaptive FE analysis of elastoplastic nonhomogeneous soil with large deformation. Comput. Geotech. 23 (1-2), 61-83. https://doi.org/10.1016/S0266-352X(98)00012-3.

Hvorslev, M.J., 1951. Time lag and soil permeability in ground-water observations. Bulletin No. 36. Waterways Experiment Station, Corps of Engineers, U.S. Army.

Maitra, S., Chatterjee, S., Choudhury, D., 2016. Generalized framework to predict undrained uplift capacity of buried offshore pipelines. Can. Geotech. J. 53 (11), 1841-1852. https://doi.org/10.1139/cgj-2016-0153.

Maitra, S., Chatterjee, S., Choudhury, D., 2017. Effect of pipe-soil interface roughness on undrained uplift capacity of buried offshore pipelines. In: Proceedings of the 27th International Ocean and Polar Engineering Conference. Paper ISOPE-I-17-244, International Society of Offshore and Polar Engineers, June 25-30, San Francisco, USA.

Maitra, S., White, D., Chatterjee, S., Choudhury, D., 2019. Numerical modelling of seepage and tension beneath plate anchors. Comput. Geotech. 108, 131-142. https://doi.org/10.1016/j.compgeo.2018.12.022.

Mana, D.S.K., Gourvenec, S., Randolph, M.F., 2014. Numerical modelling of seepage beneath skirted foundations subjected to vertical uplift. Comput. Geotech. 55, 150-157. https://doi.org/10.1016/j.compgeo.2013.08.007.

Martin, C.M., Randolph, M.F., 2006. Upper bound analysis of lateral pile capacity in cohesive soil. Géotechnique 56 (2), 141-145. https://doi.org/10.1680/geot.2006.56.2.141.

Martin, C.M., White, D.J., 2012. Limit analysis of the undrained bearing capacity of offshore pipelines. Géotechnique 62 (9), 847–863. https://doi.org/10.1680/geot.12.OG.016.

Palmer, A.C., Ellinas, C.P., Richards, D.M., Guijt, J., 1990. Design of submarine pipelines against upheaval buckling. In: Proceedings of the Offshore Technology Conference. Houston, Texas, USA. https://doi.org/10.4043/6335-MS.

Randolph, M.F., Houlsby, G.T., 1984. The limiting pressure on a circular pile loaded laterally in cohesive soil. Géotechnique 34 (4), 613-623. https://doi.org/10.1680/geot.1984.34.4.613.

Ratnam, S., Soga, K., Whittle, R.W., 2001. Revisiting Hvorslev's intake factors using the finite element method. Géotechnique 51 (7), 641-645. https://doi.org/10.1680/geot.2001.51.7.641.

Thieken, K., Achmus, M., Schröder, C., 2014. On the behavior of suction buckets in sand under tensile loads. Comput. Geotech. 60, 88-100. https://doi.org/10.1016/j.compgeo.2014.04.004.

Thusyanthan, N.I., Ganesan, S.A., Bolton, M.D., Allan, P., 2008. Upheaval buckling resistance of pipelines buried in clayey backfill. In: Proceedings of the Eighteenth International Offshore and Polar Engineering Conference, Vancouver, B.C., Vol. 2, pp. 174–180.

Valle-Molina, C., Alamilla, J.L., Sánchez-Moreno, J., Najjar, S.S., López-Acosta, N.P., 2014. Reliability functions for buried submarine pipelines in clay subjected to upheaval buckling. Appl. Ocean Res. 48, 308-321. https://doi.org/10.1016/j.apor.2014.10.004.

Wilkinson, W.B., 1968. Constant head in situ permeability tests in clay strata. Géotechnique 18 (2), 172-194. https://doi.org/10.1680/geot.1968.18.2.172.

Zeng, X., Duan, M., Che, X., 2014. Critical upheaval buckling forces of imperfect pipelines. Appl. Ocean Res. 45, 33-39. https://doi.org/10.1016/j.apor.2014.01.001.

Zhou, H., Randolph, M.F., 2007. Computational techniques and shear band development for cylindrical and spherical penetrometers in strain-softening clay. Int. J. Geomech. 7 (4), 287-295. https://doi.org/10.1061/(ASCE)1532-3641(2007)7:4(287).

**Table 1 Design example on buckling behaviour of buried pipe for $\Delta T$ = 70°C**

| **Parameters** | **Values** |
|---|---|
| *Pipe properties:* | |
| Diameter, $D$ | 350 mm |
| Wall thickness | 20 mm |
| Submerged operational weight, $W'$ | 1.2 kN/m |
| Young's modulus, $E$ | 210 GPa |
| Initial embedment ratio of pipe, $w/D$ | 3 |
| Height of imperfection, $\delta$ | 0.25 m |
| Length of imperfection, $L$ | 15 m |
| Interface roughness coefficient | 0.5 |
| | |
| *Soil properties:* | |
| Shear strength of soil (where, $z$ is depth in metres) | 1.5$z$ kPa |
| Submerged unit weight, $\gamma'$ | 4 kN/m$^3$ |
| Permeability, $k$ | $10^{-8}$ m/s |
| | |
| *Expansion effect:* | |
| Thermal expansion coefficient | $1.2\times10^{-5}$ / °C |
| Operational temperature (in excess of in-situ temperature), $\Delta T$ | 70° C |
| | |
| *Derived parameters:* | |
| Flexural rigidity of pipe, $EI$ | 59.49 MNm$^2$ |
| Thermal strain | $8.4\times10^{-4}$ / °C |
| Thermal stress | 176.4 MPa |
| Thermal compressive force, $P$ | 3.658 MN |
| | |
| *Check against upheaval buckling:* | |
| Dimensionless imperfection length, $\phi_L$ (from Eq. 8) | 3.72 |
| Maximum download parameter, $\phi_w$ obtained from universal design curve by Palmer et al. (1990) (see Fig. 12) | 0.0646 |
| Required uplift resistance to prevent buckling, $V$ (using Eq. 7) | 3.63 kN/m |

**Figure Captions**

**Fig. 1** Problem geometry and notation

**Fig. 2** Typical finite element mesh showing the FE model with gap elements for buried pipes ($w/D = 2$)

**Fig. 3** Comparison of obtained uplift factors ($N_u$) at $v/k = 0.01$ and $10^4$ with NT and FT uplift factors respectively in weightless soil

**Fig. 4** Uplift response for $D = 1$ m: (a) Mobilisation of uplift resistance with pipe displacement for $w/D = 2$, $\gamma'D/s_u = 0$; (b) Mobilisation of uplift resistance with pipe displacement for $w/D = 4$, $\gamma'D/s_u = 0$; (c) $N_u$ versus $v/k$ for $w/D = 2$, $\gamma'D/s_u = 0, 1, 2$; and (d) $N_u$ versus $v/k$ for $w/D = 4$, $\gamma'D/s_u = 0, 1, 2$ (letter markers indicate the corresponding sub-figure in Figs. 5 and 6)

**Fig. 5** Uplift mechanisms of buried pipes for $w/D = 2, 4$; $\gamma'D/s_u = 0, 2$; and $v/k = 10, 100$ ($s_u = 10$ kPa, $D = 1$ m)

**Fig. 6** Excess pore pressure contours for $w/D = 2, 4$; $v/k = 10, 100$; and $\gamma'D/s_u = 0, 2$ ($s_u = 10$ kPa, $D = 1$ m)

**Fig. 7** Estimation of interface tension using Hvorslev's intake factor, $F$ for (a) $w/D = 2$, $D = 1$ m, $s_u = 10$, 20 and 40 kPa; (b) $w/D = 2$, $D = 0.5$ m, $s_u = 10$, 20 and 40 kPa; (c) $w/D = 1.5, 2, 3, 4, 5$; $s_u = 10$ kPa, $\gamma' = 0$

**Fig. 8** Variation of intake factor, $F$ with $w/D$

**Fig. 9** Normalised uplift capacity ($V_u/s_{u0}D$) at various uplift rates for $\mu = 0, 0.05, 0.1$ and $0.2$: (a) $w/D = 2$, (b) $w/D = 4$ ($s_{u0} = 10$ kPa, $D = 1$ m, $\gamma' = 0$, $k = 10^{-7}$ m/s, $\dot{\gamma}_{ref} = 3 \times 10^{-6}$ s$^{-1}$)

**Fig. 10** Normalisation of obtained uplift capacities with $s_{u,eff}D$ for $w/D = 1.5, 2, 3, 4, 5$ and $\mu = 0, 0.05, 0.1, 0.2$ ($s_{u0} = 10$ kPa, $D = 1$ m, $\gamma' = 0$, $k = 10^{-7}$ m/s, $\dot{\gamma}_{ref} = 3 \times 10^{-6}$ s$^{-1}$)

**Fig. 11** Mechanical analogue system to represent uplift with seepage

**Fig. 12** Application of universal design curve proposed by Palmer et al. (1990) to predict upheaval buckling behaviour ($\Delta T = 70°$ C)

**Fig. 13** Prediction of buckling behaviour for a pipe in operation: (a) Variation in embedment ratio over time, (b) Variation in uplift velocity over time

Figure_1

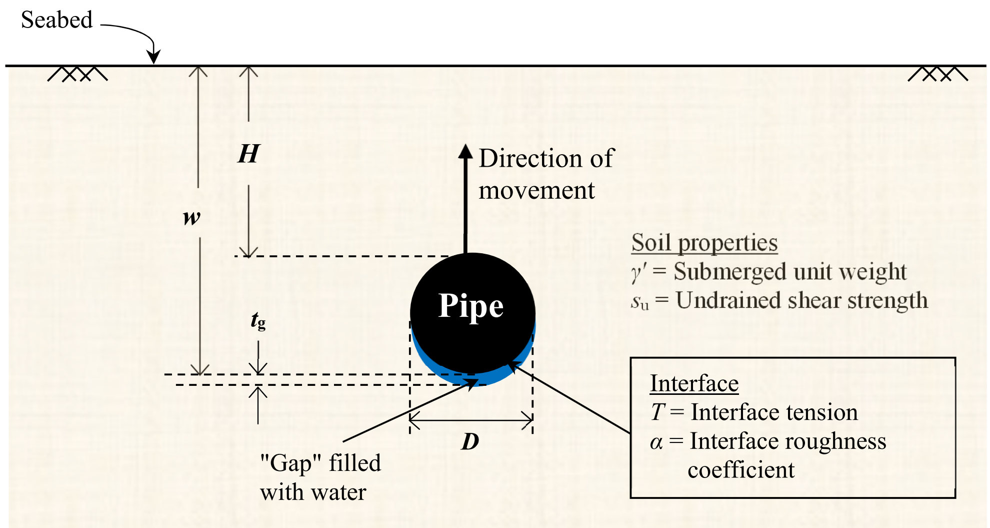

Seabed
H
w
Direction of movement
Soil properties
γ′ = Submerged unit weight
$s_u$ = Undrained shear strength
Pipe
$t_g$
Interface
T = Interface tension
α = Interface roughness coefficient
D
"Gap" filled with water

Figure_2

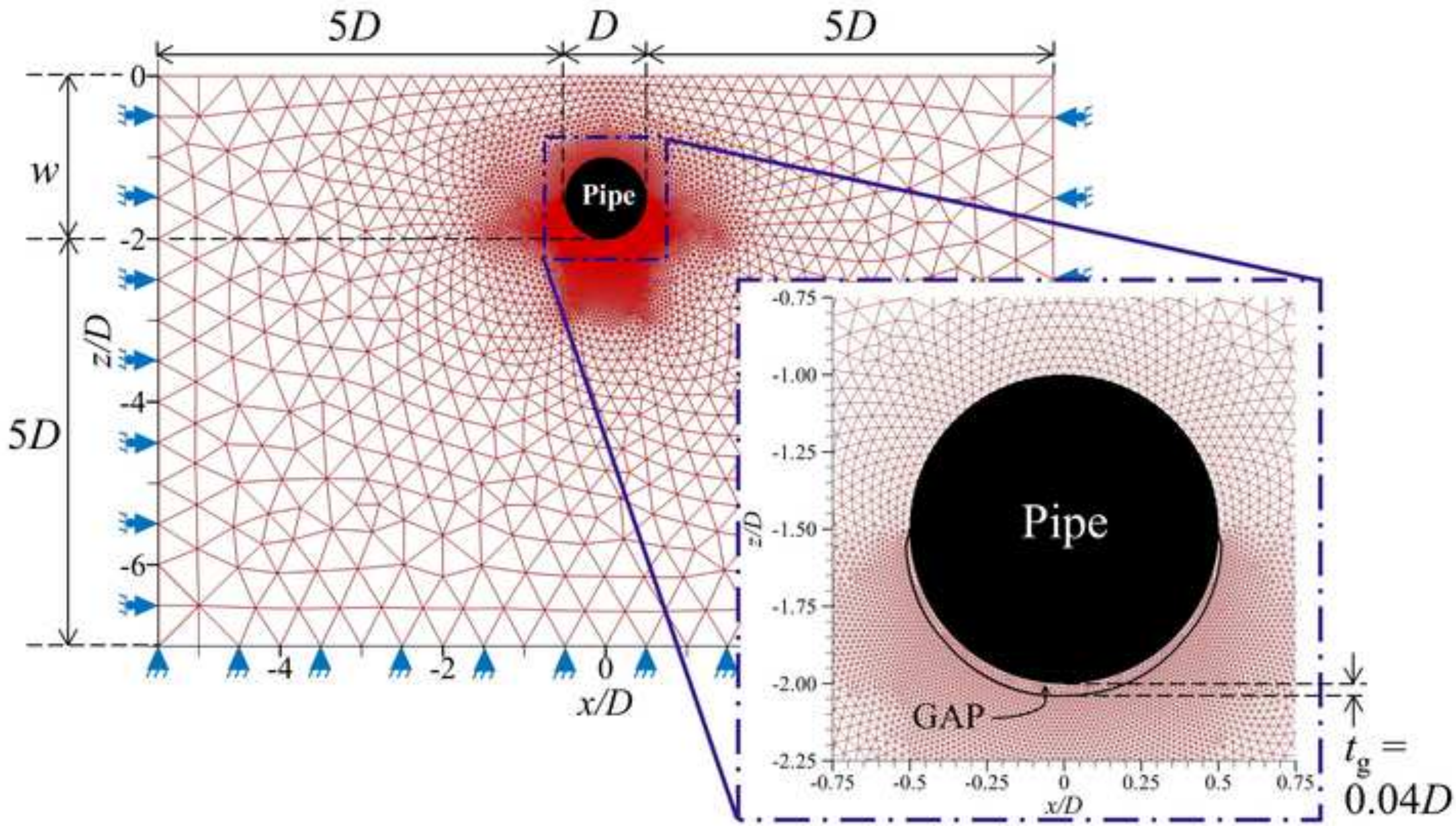

5D
D
5D
w
5D
Pipe
z/D
x/D
0
-2
-4
-6
-4
-2
0
-0.75
-1.00
-1.25
-1.50
-1.75
-2.00
-2.25
-0.75
-0.5
-0.25
0
0.25
0.5
0.75
Pipe
GAP
$t_g$ =
0.04D

Figure_3

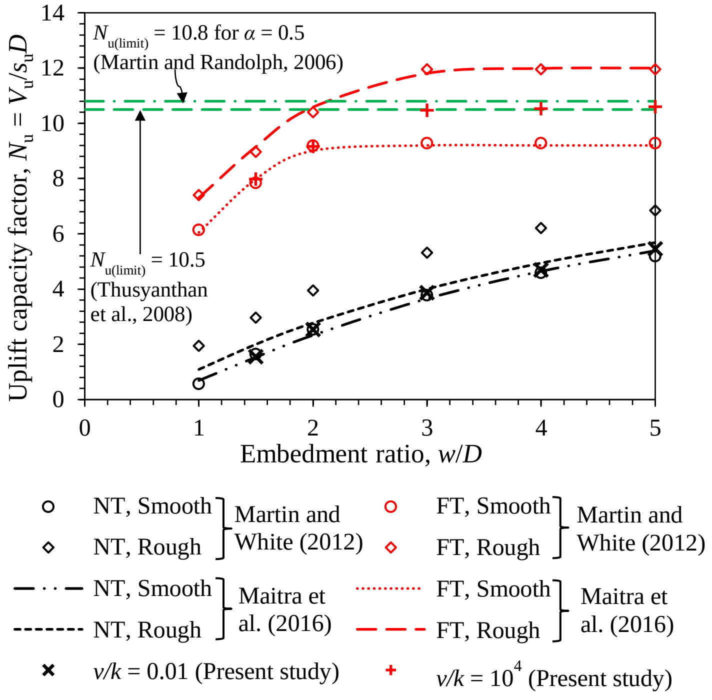

14
12
10
8
6
4
2
0
0
1
2
3
4
5
Uplift capacity factor, $N_u = V_u/s_uD$
Embedment ratio, $w/D$
$N_{u(limit)}$ = 10.8 for $\alpha$ = 0.5
(Martin and Randolph, 2006)
$N_{u(limit)}$ = 10.5
(Thusyanthan et al., 2008)
NT, Smooth
NT, Rough
Martin and White (2012)
FT, Smooth
FT, Rough
Martin and White (2012)
NT, Smooth
NT, Rough
Maitra et al. (2016)
FT, Smooth
FT, Rough
Maitra et al. (2016)
$v/k$ = 0.01 (Present study)
$v/k = 10^4$ (Present study)

Figure_4

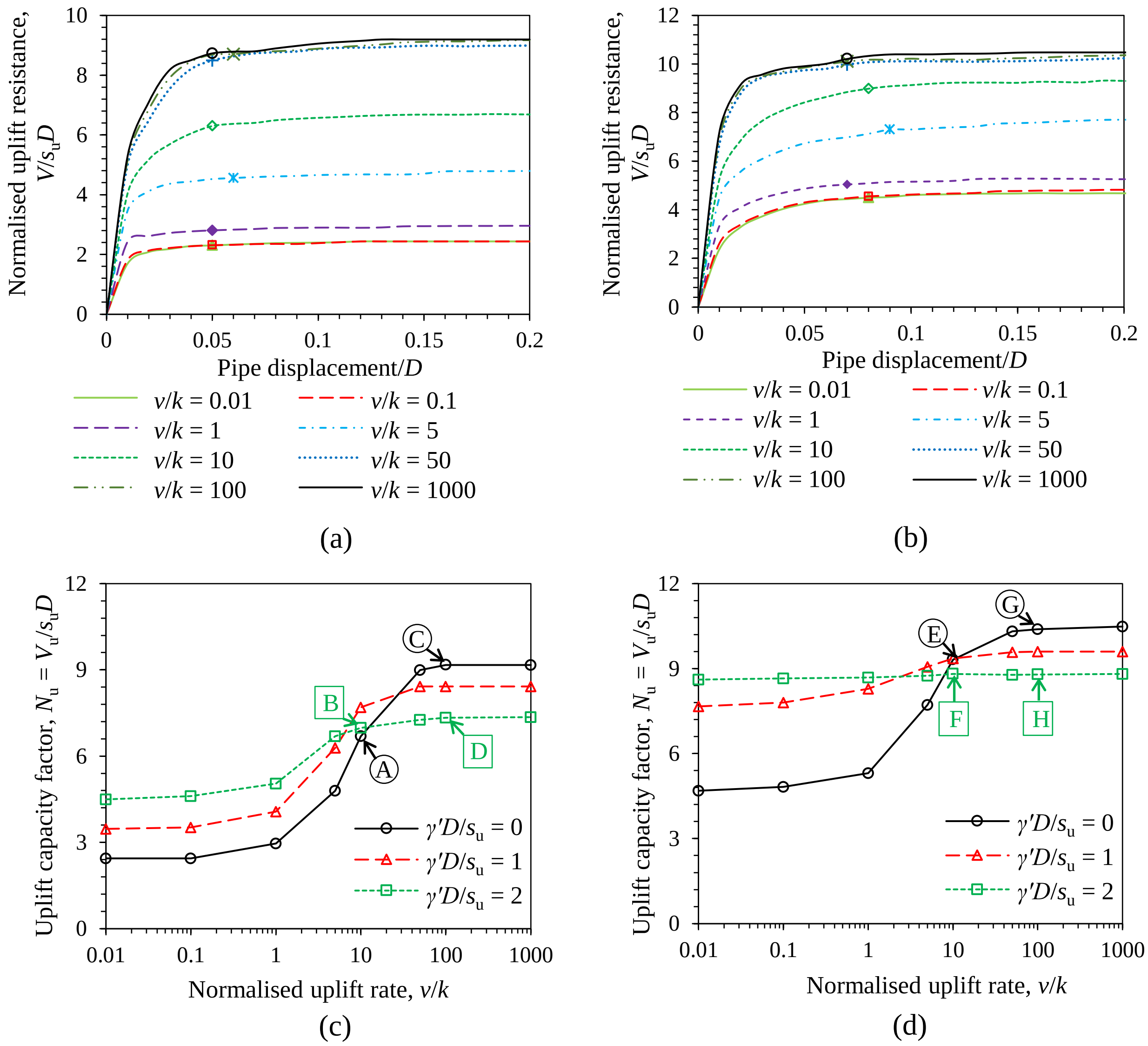

Normalised uplift resistance, $V/s_uD$
Pipe displacement/$D$
$v/k$ = 0.01
$v/k$ = 0.1
$v/k$ = 1
$v/k$ = 5
$v/k$ = 10
$v/k$ = 50
$v/k$ = 100
$v/k$ = 1000
(a)
(b)
Uplift capacity factor, $N_u = V_u/s_uD$
Normalised uplift rate, $v/k$
$\gamma'D/s_u$ = 0
$\gamma'D/s_u$ = 1
$\gamma'D/s_u$ = 2
A
B
C
D
E
F
G
H
(c)
(d)

Figure_5

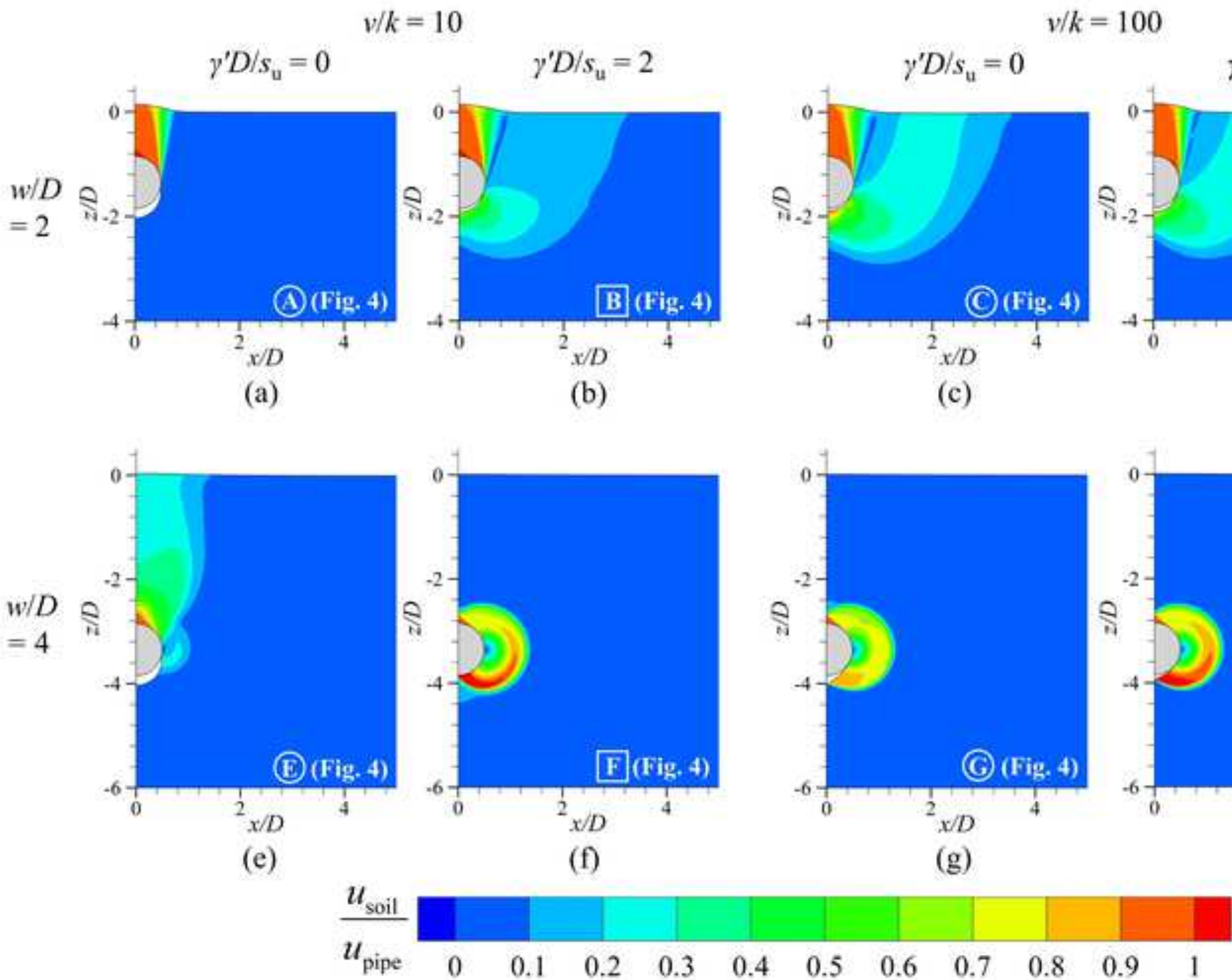

v/k = 10
v/k = 100
γ'D/s_u = 0
γ'D/s_u = 2
γ'D/s_u = 0
γ'D/s_u = 2
w/D = 2
w/D = 4
z/D
x/D
A (Fig. 4)
B (Fig. 4)
C (Fig. 4)
D (Fig. 4)
E (Fig. 4)
F (Fig. 4)
G (Fig. 4)
H (Fig. 4)
(a)
(b)
(c)
(d)
(e)
(f)
(g)
(h)
u_soil / u_pipe
0
0.1
0.2
0.3
0.4
0.5
0.6
0.7
0.8
0.9
1

Figure_6

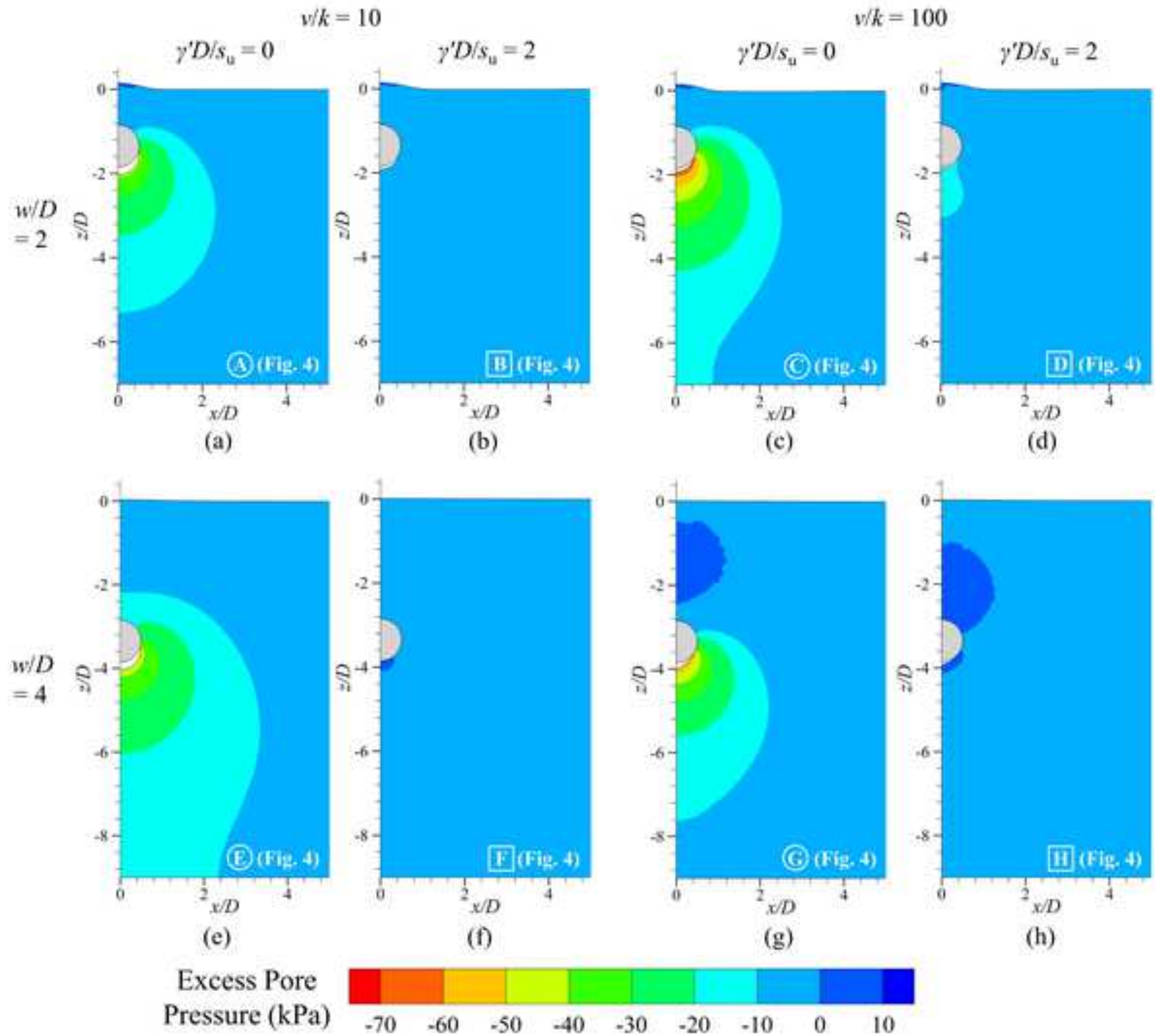

v/k = 10
v/k = 100
γ'D/s_u = 0
γ'D/s_u = 2
γ'D/s_u = 0
γ'D/s_u = 2
w/D = 2
w/D = 4
z/D
x/D
A (Fig. 4)
B (Fig. 4)
C (Fig. 4)
D (Fig. 4)
E (Fig. 4)
F (Fig. 4)
G (Fig. 4)
H (Fig. 4)
(a)
(b)
(c)
(d)
(e)
(f)
(g)
(h)
Excess Pore Pressure (kPa)
-70 -60 -50 -40 -30 -20 -10 0 10

Figure_7

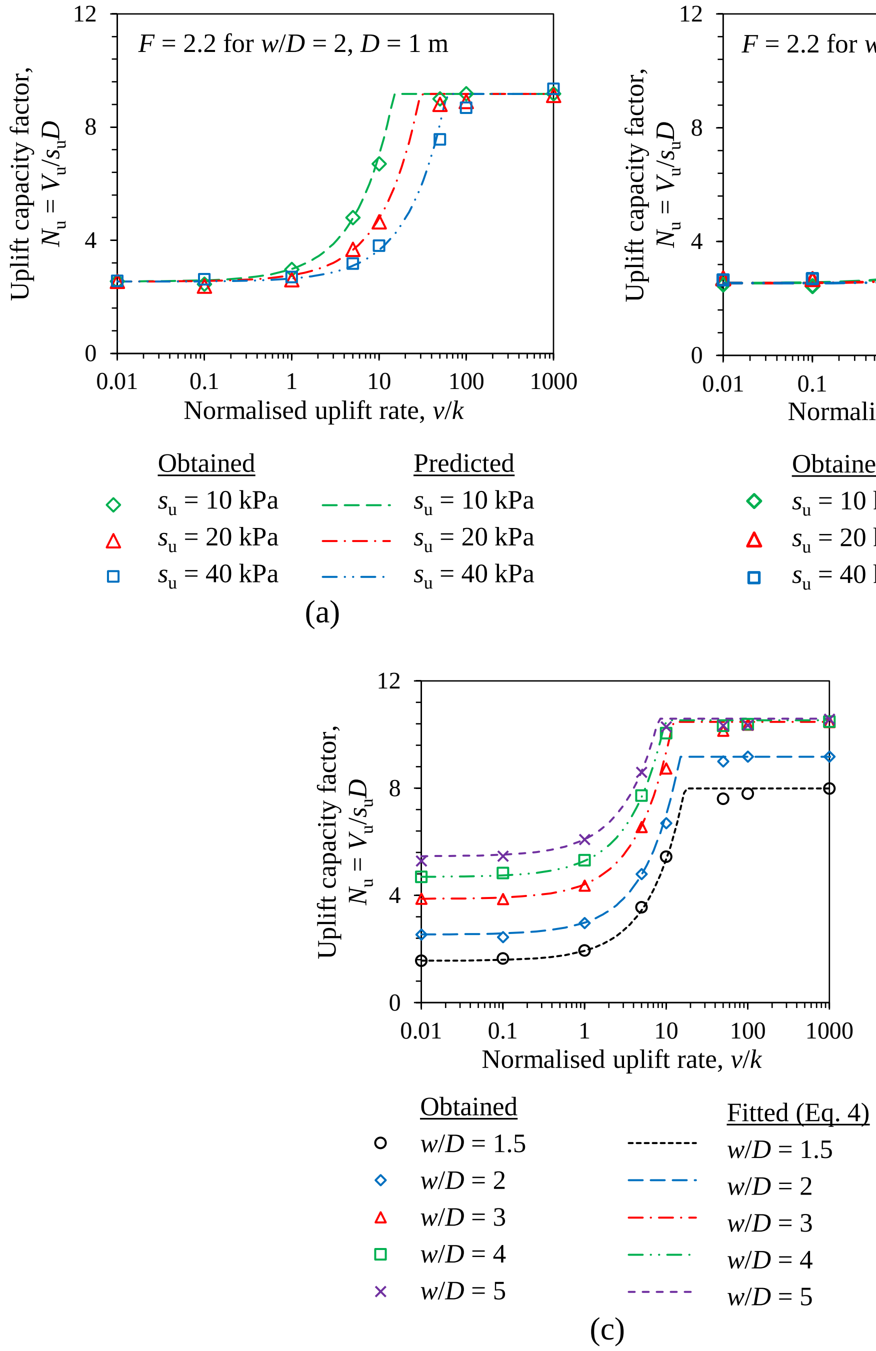

F = 2.2 for w/D = 2, D = 1 m
Uplift capacity factor, N_u = V_u/s_uD
Normalised uplift rate, v/k
Obtained
Predicted
s_u = 10 kPa
s_u = 20 kPa
s_u = 40 kPa
(a)
F = 2.2 for w/D = 2, D = 0.5 m
(b)
Fitted (Eq. 4)
w/D = 1.5
w/D = 2
w/D = 3
w/D = 4
w/D = 5
(c)

Figure_8

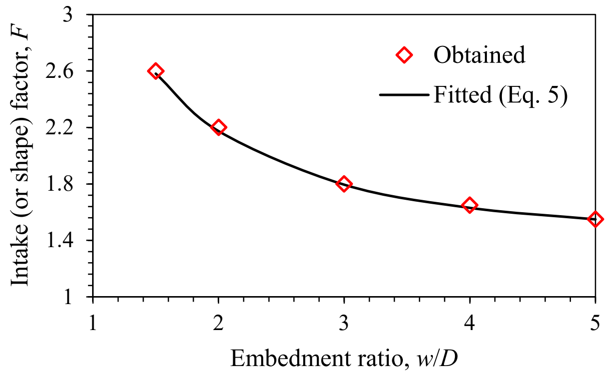

Intake (or shape) factor, F
Embedment ratio, w/D
Obtained
Fitted (Eq. 5)
3
2.6
2.2
1.8
1.4
1
1
2
3
4
5

Figure_9

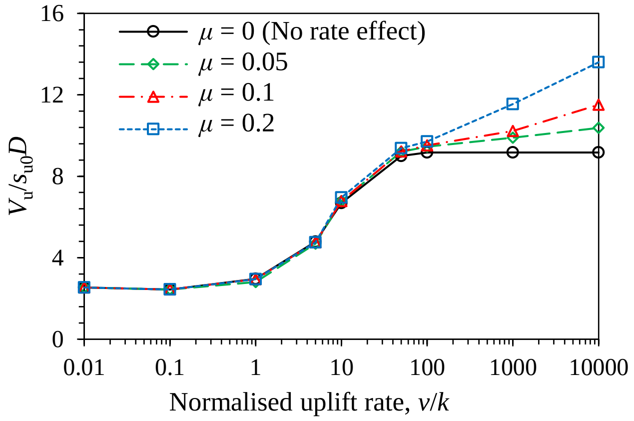

16
12
8
4
0
$V_u/s_{u0}D$
0.01
0.1
1
10
100
1000
10000
Normalised uplift rate, $v/k$
$\mu$ = 0 (No rate effect)
$\mu$ = 0.05
$\mu$ = 0.1
$\mu$ = 0.2


(a)

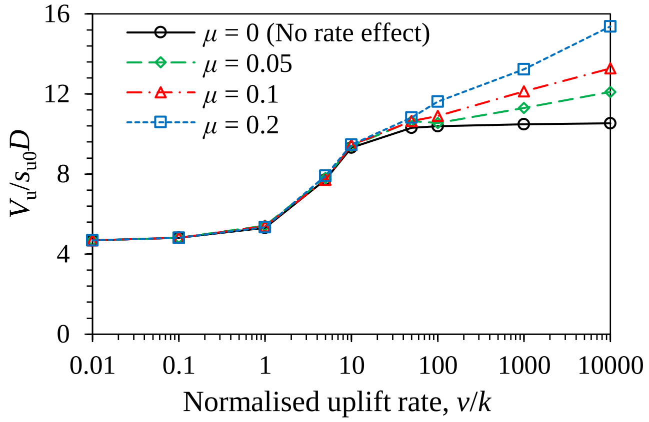

16
12
8
4
0
$V_u/s_{u0}D$
0.01
0.1
1
10
100
1000
10000
Normalised uplift rate, $v/k$
$\mu$ = 0 (No rate effect)
$\mu$ = 0.05
$\mu$ = 0.1
$\mu$ = 0.2


(b)

Figure_10

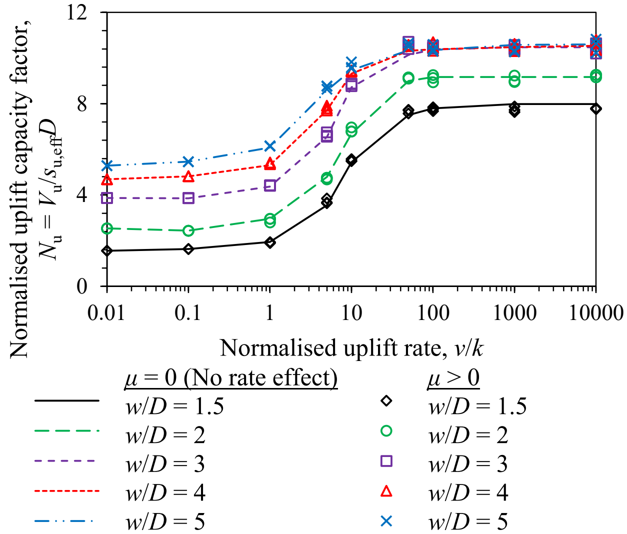

12
8
4
0
0.01
0.1
1
10
100
1000
10000
Normalised uplift capacity factor, $N_u = V_u/s_{u,eff}D$
Normalised uplift rate, $v/k$
$\mu$ = 0 (No rate effect)
$w/D$ = 1.5
$w/D$ = 2
$w/D$ = 3
$w/D$ = 4
$w/D$ = 5
$\mu$ > 0
$w/D$ = 1.5
$w/D$ = 2
$w/D$ = 3
$w/D$ = 4
$w/D$ = 5

Figure_11

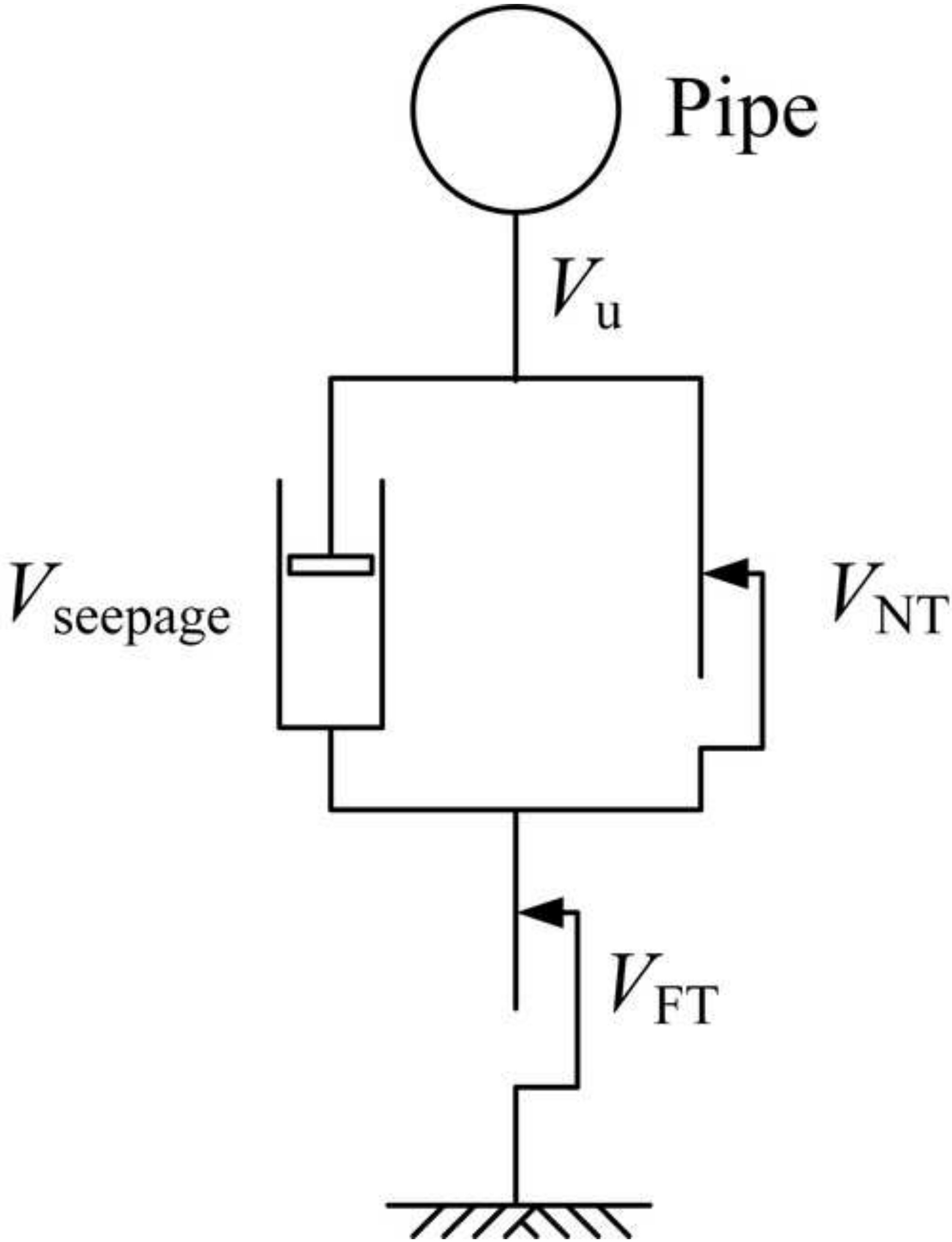

Figure_12

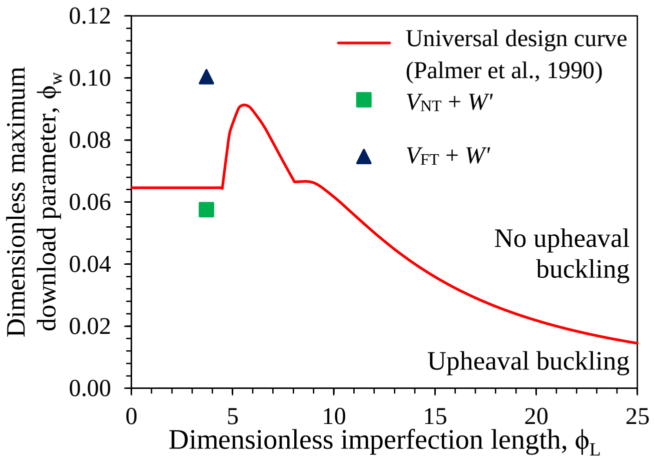

Universal design curve
(Palmer et al., 1990)
$V_{NT} + W'$
$V_{FT} + W'$
No upheaval
buckling
Upheaval buckling
0.12
0.10
0.08
0.06
0.04
0.02
0.00
Dimensionless maximum
download parameter, $\phi_w$
0
5
10
15
20
25
Dimensionless imperfection length, $\phi_L$

Figure_13

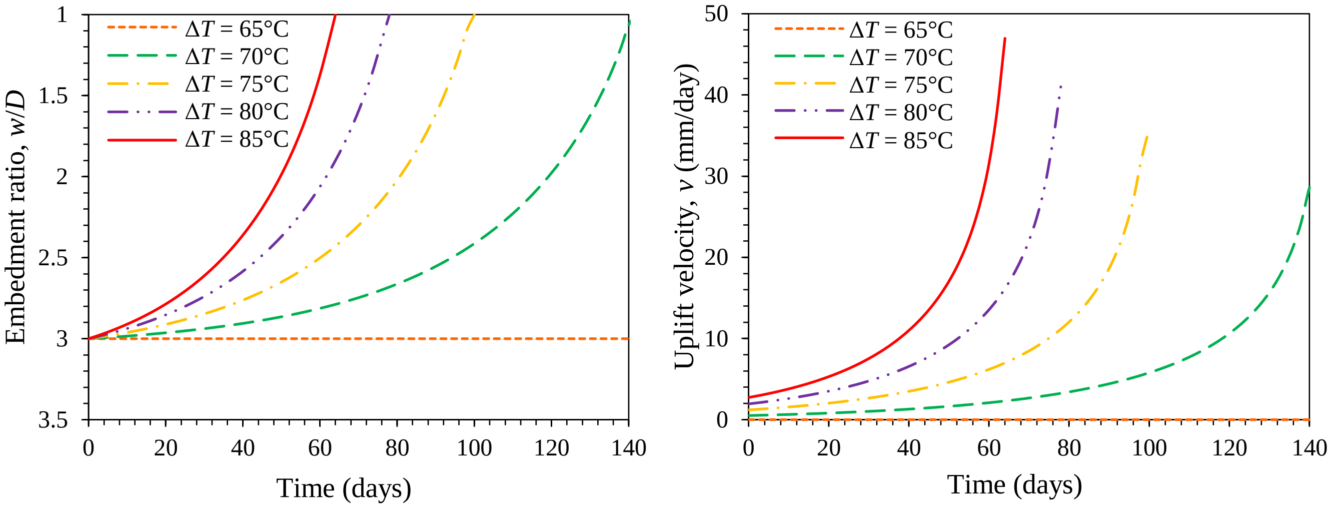

ΔT = 65°C
ΔT = 70°C
ΔT = 75°C
ΔT = 80°C
ΔT = 85°C
Embedment ratio, w/D
1
1.5
2
2.5
3
3.5
0
20
40
60
80
100
120
140
Time (days)
ΔT = 65°C
ΔT = 70°C
ΔT = 75°C
ΔT = 80°C
ΔT = 85°C
Uplift velocity, v (mm/day)
50
40
30
20
10
0
0
20
40
60
80
100
120
140
Time (days)


(a)

(b)